Experimental Results of 144-Element Dual-Polarized Endfire Tapered-Slot Phased Arrays

Henrik Holter, Tan-Huat Chio, *Member, IEEE,* and Daniel H. Schaubert, *Fellow, IEEE*

***Abstract*—Two $9 \times 8 \times 2$ (144 element) dual-polarized endfire tapered-slot phased arrays have been built. Measured data for mutual coupling coefficients and scan-element patterns are presented. Also, element resonances, predicted by numerical infinite-array analysis are examined. The dimensions of the two arrays are identical. They differ in that plated-through vias have been repositioned to eliminate element resonances. One array was expected to operate from 1.0 to 4.6 GHz and the other from 1.0 to 5.9 GHz. It was found that, at low frequencies, the central elements are heavily affected by the finiteness of the arrays due to strong mutual coupling between array elements. Extrapolation of the observations indicates that a tapered-slot phased array, designed for wide-angle scanning, should be comprised of at least 30–40 rows and columns of elements to obtain low-frequency performance that is comparable to infinite-array predictions. In spite of the smallness of the array, predicted-element resonances could be identified by examination of the phase of the mutual coupling coefficients. Based on these observations, the plated-through vias are adequate to remove element resonances.**

***Index Terms*—Broad-band phased array, measurement, mutual coupling, tapered slot phased array.**

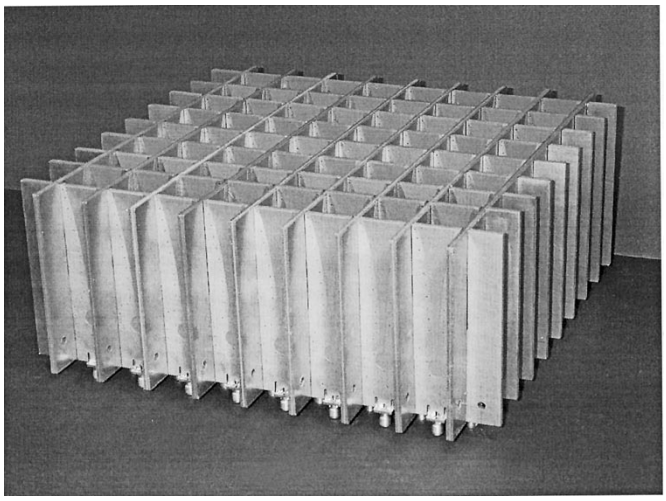

Fig. 1. Prototype array comprised of nine printed circuit cards for each polarization, eight tapered slot elements per card. The element spacing is 27.02 mm (0.09λ at 1.0 GHz) in the x- and y-direction in both arrays.

I. Introduction

THE TAPERED-SLOT element is a promising candidate for both single- and dual-polarized wide-band and wide-angle scanning phased arrays. Numerical calculations of infinite arrays have shown that a bandwidth of $5.9:1$ over a scan volume of $\pm 50^0$ is achievable. Scan blindness and resonances limit the upper frequency band. The element spacing at the lowest frequencies can be as small as 0.1 wavelengths, which means that the effect of mutual coupling between array elements is extremely important. Finite-array behavior is therefore of great interest. The complex geometry of the tapered-slot element makes finite-array analysis exceptionally time consuming. Both single- and dual-polarized finite tapered-slot arrays with different types and numbers of elements have been built earlier [1]–[4]. The array in [2] contains more than 4000 discrete radiating elements. The purpose of this paper is to present measured results for two finite dual-polarized tapered-slot phased arrays, designed by full-wave analysis. The full-wave analysis was performed in MoM and FDTD by considering a unit cell in an infinite array. Parameter studies that led to the array design are presented in [5]. The arrays are identical except that one array contains "contoured" vias rather than straight vias. The contoured vias are intended to eliminate band-limiting resonances. Measured data of mutual coupling coefficients and scan-element patterns are presented. The measured scan-element patterns are compared with scan-element patterns calculated from the mutual coupling coefficients. Also, predicted element resonances are identified by examination of the phase of the mutual coupling coefficients. Additional coupling data and co- and cross-polarized scan-element patterns and design information can be found in [6].

Manuscript received July 13, 1999; revised June 6, 2000. This work was supported in part by NFRA/ASTRON, Dwingeloo, the Netherlands, the Royal Institute of Technology, Stockholm, and the University of Massachusetts, Amherst.

H. Holter is with the Division of Electromagnetic Theory, Royal Institute of Technology, SE-100 44 Stockholm, Sweden.

T-H. Chio was with the University of Massachusetts, Amherst, MA 01003 USA. He is now with the DSO National Laboratories, Singapore, 118230 Republic of Singapore.

D. H. Schaubert is with the Department of Electrical and Computer Engineering, University of Massachusetts, Amherst, MA 01003 USA.

Publisher Item Identifier S 0018-926X(00)07715-2.

II. Array Geometry

One of the dual-polarized arrays is shown in Fig. 1. The two arrays are comprised of the elements shown as insets in Figs. 2 and 3. The dimensions of the two arrays are identical. They differ in that plated-through vias have been repositioned to eliminate element resonances. The element spacing is 27.02 mm (0.09λ at 1.0 GHz) in the x- and y-direction. The elements consist of a slotline and a slotline cavity etched in metal fins on each side of a dielectric substrate. A stripline terminated in a stripline stub is located between the metal fins and feeds the element. The exponential opening of the slotline is determined by $R = 0.03$ mm^{-1} [5]. The dual-polarized array is designed by positioning the elements in a square lattice as shown in Fig. 1. Each array consists of 144 elements. Metal walls or plated-through vias

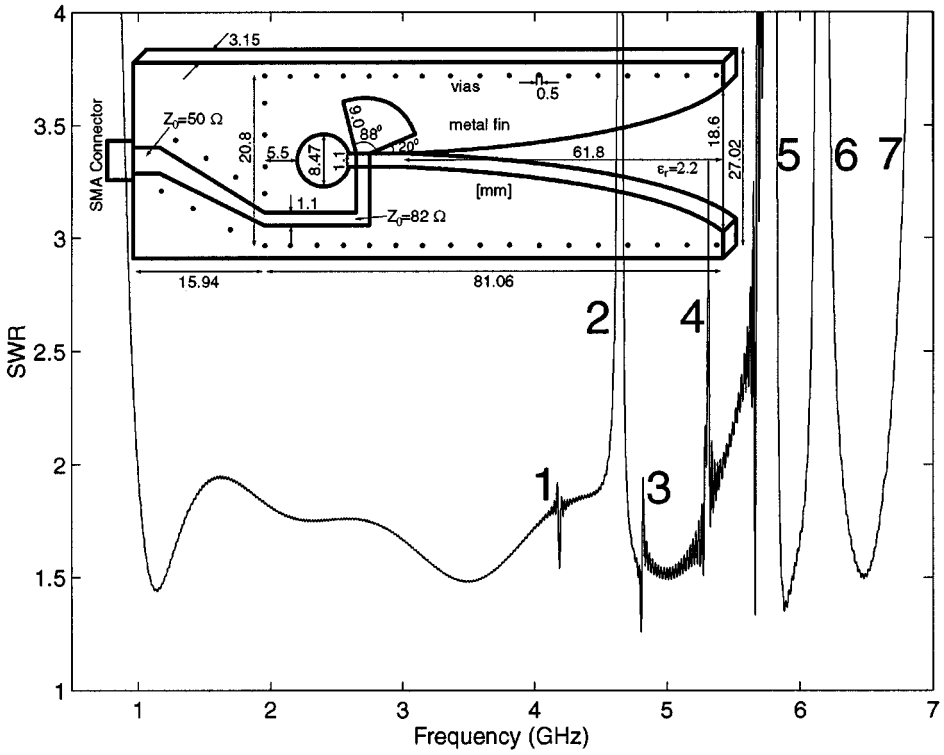

Fig. 2. Numerically calculated SWR for an infinite array comprised of "straight" via elements scanned to 50^0 in the H-plane. The first grating lobe appears at 6.29 GHz.

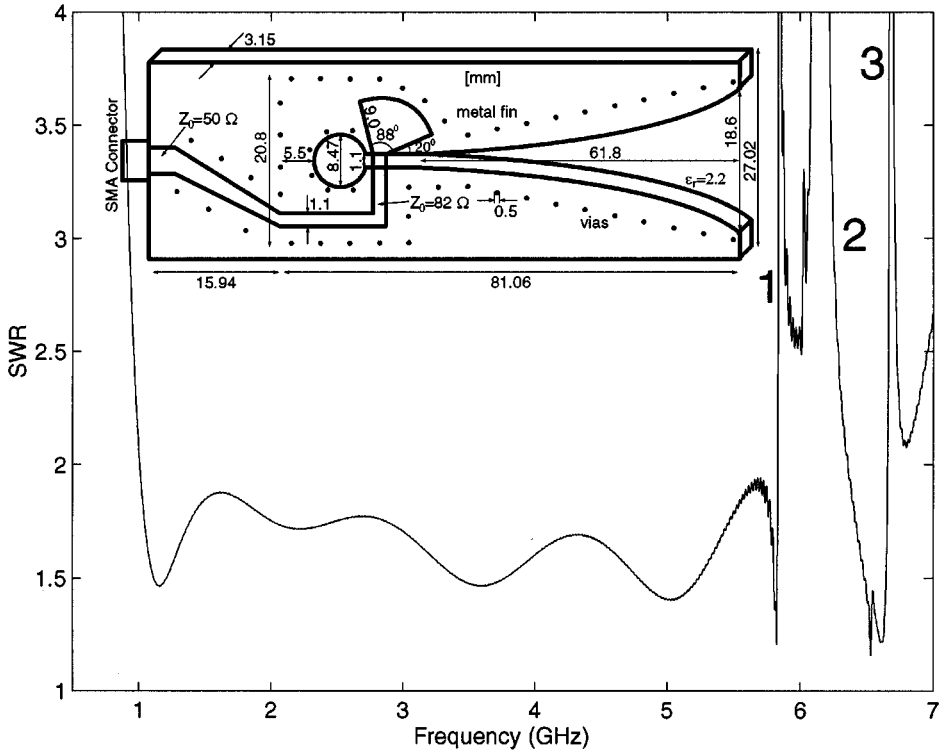

Fig. 3. Numerically calculated SWR for an infinite array comprised of "contour" via elements scanned to 50^0 in the H-plane. The first grating lobe appears at 6.29 GHz.

must be positioned in the dielectric substrate where the orthogonal elements intersect, as shown in Fig. 2. Otherwise, numerical simulations of infinite arrays have shown that several strong resonances will appear in the intended frequency band of oper-

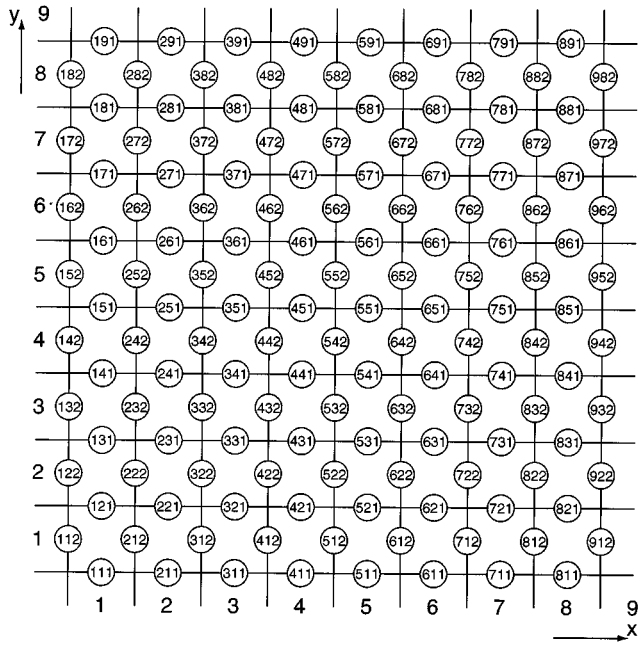

Fig. 4. Array back view. Numbering of connectors.

ation. An alternative way of positioning the vias is shown in Fig. 3. No ground plane is needed behind the array since the waveguides formed in the air spaces between the elements in Fig. 1 are far below cutoff. Numerical simulations of elongated elements have verified this. The elements in the array are numbered as shown in Fig. 4 with three indexes representing column, row, and polarization. For example, connector 542 is for a vertical or y-directed element near the center of the array.

The array comprised of elements shown in Fig. 2 will be called the straight via array and the array comprised of elements shown in Fig. 3 will be called the contour via array. Numerical simulations show that the contoured vias eliminate several resonances or impedance anomalies at the upper end of the operating band.

III. Identification of Element Resonances

Scan blindness and resonances limit the upper frequency band of tapered slot phased arrays. The resonances are especially serious for scanning in the H-plane. Fig. 2 shows calculated SWR for an infinite array comprised of straight via elements when the array is scanned to 50^0 in the H-plane. The calculation is performed with the finite-difference time-domain method by considering a unit cell in an infinite array [7], [8]. The resonances have earlier been found to be related to the cavity formed by the dielectric region of the tapered slot element, and can be eliminated or reduced in all scan planes by plated-through vias in the elements as shown in Fig. 3 [9]. It is well known that it can be difficult to observe phenomena such as scan blindness and resonances, predicted by numerical calculations of infinite arrays, in small finite arrays. This was true for both tapered-slot arrays. Neither the input impedance nor the scan-element pattern reveals obvious resonances at the predicted frequencies. However, the phase of the mutual coupling coefficients is sensitive to these anomalies. Figs. 5 and 6 show the phase of the mutual coupling coefficients (scattering parameters) between different elements as a function of frequency. The numbered arrows in Figs. 5 and 6 correspond to the locations of the resonances in Figs. 2 and 3. The behavior of the phase is quite smooth for frequencies below the first arrow, corresponding to the first resonance. However, aberrations appear in the vicinity of the predicted resonances. Since the only difference between the two arrays is the via configuration, the difference in the phase behavior between the arrays is most likely caused by the resonances. This verifies to some extent the examination of impedance anomalies in [9].

IV. Coupling Coefficients

The magnitude of the mutual coupling coefficients $|S_{12}|$ is presented only for the straight via array. Similar results were obtained for the array with contoured vias. The information is presented in the form of contour plots. The mutual coupling coefficients are always measured between element 542 (Fig. 4) and another element. Since element 542 is not the central element, all plots show an asymmetry.

Figs. 7–10 show the magnitude of the mutual coupling coefficients in a logarithmic scale for the central column and row in the array as a function of frequency. Figs. 7 and 9 show coupling along a vertical column of the array (nominally the E-plane of element 542). Figs. 8 and 10 show coupling along a horizontal row. The similarities of Figs. 7 and 8 and of 9 and 10 indicate that the coupling mechanism is similar in the principal planes. The coupling in Figs. 7 and 8 shows some tendency to decay more rapidly with distance at higher frequencies. A similar trend may be present in Figs. 9 and 10, though the coupling is altered near 1.5 GHz and above 4.5 GHz, where resonances and anomalies are predicted for H-plane scanning. Figs. 11–13 show the magnitude of the coupling coefficients in a logarithmic scale between element 542 and all vertical elements at 1.5, 3.5, and 5.5 GHz. Figs. 14–16 show the coupling between element 542 and all horizontal elements at these frequencies. These plots show how the coupling coefficients decay at specific frequencies. Consider, for example, the coupling coefficients between element 542 and all vertical elements at 3.5 GHz in Fig. 12. The magnitude of the coupling coefficients is about -30 dB for the outermost elements. But there are 30 vertical elements in the outer perimeter of the array. The contribution to the scan-reflection coefficient for element 542 from all these elements could be significant if all mutual coupling coefficients added in phase. Usually, they will not add in phase, but this shows that the effect of mutual coupling between distant elements is important in tapered-slot phased arrays and that the finite size of the array, i.e., the effects of elements that are not present beyond the array perimeter, could create important differences between infinite array predictions and measured finite-array results. Figs. 11–13 also show that the coupling decays more rapidly in the principal planes than in the diagonal planes. This is true for copolarized as well as cross-polarized elements and may be related to the observed polarization characteristics of tapered-slot antennas [10], [11]

V. Scan-Element Patterns

Numerical calculations of tapered-slot arrays based on infinite-array analysis show that the scan-element pattern is very broad.

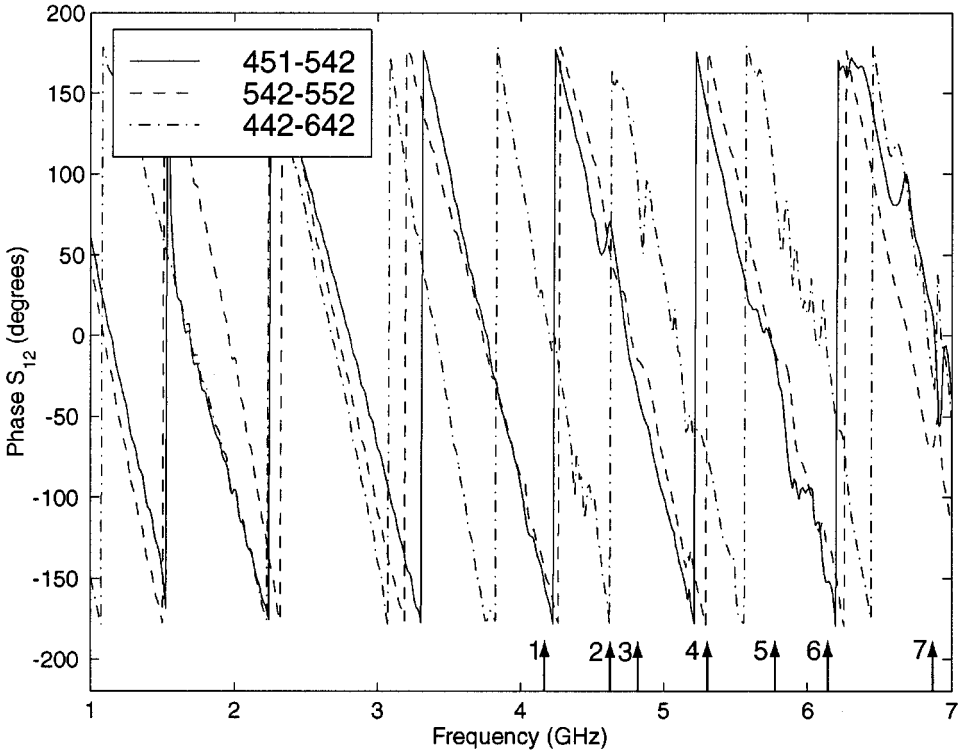

Fig. 5. Phase of mutual coupling coefficients between different elements in straight via array. The numbered arrows show the locations of the resonances in Fig. 2.

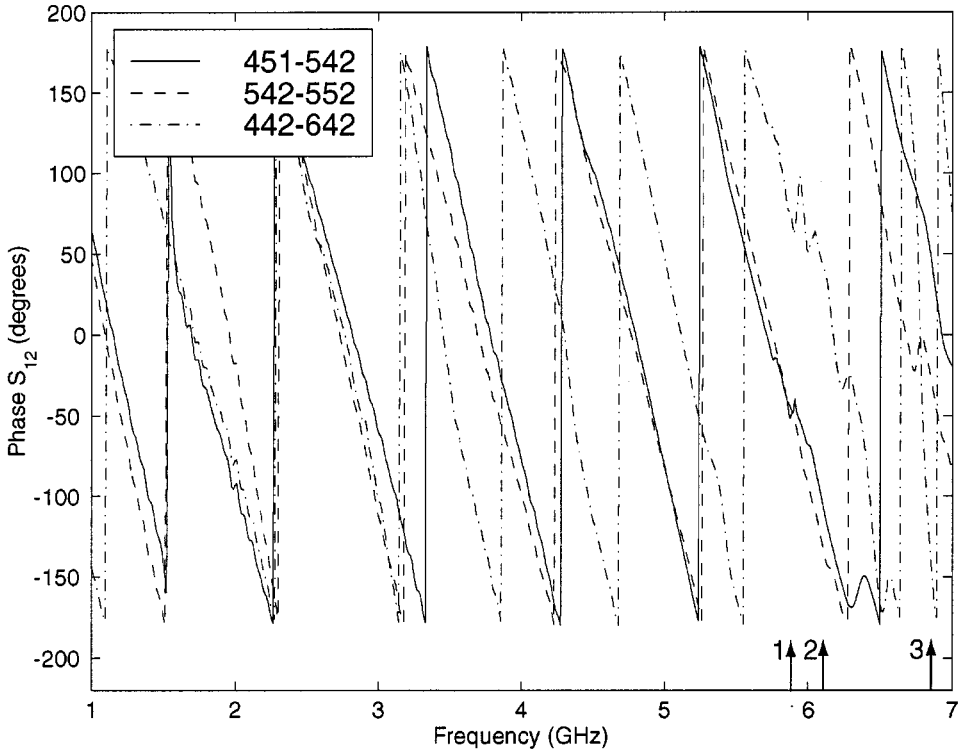

Fig. 6. Phase of mutual coupling coefficients between different elements in contoured via array. The numbered arrows show the locations of the resonances in Fig. 3.

The tapered-slot element is therefore supposed to be a good radiator for wide-angle scanning arrays. For infinite arrays, the scan element pattern $F(\theta, \varphi)$ can be calculated as [12], [13]

$$F(\theta, \varphi) = \frac{4\pi}{\lambda^2} A_e (1 - |\Gamma_S(\theta, \varphi)|^2) \cos\theta \qquad (1)$$

where A_e is the unit cell area of one element in the array, λ is the wavelength and

$$\Gamma_S(\theta, \varphi) = \sum_{m=-\infty}^{\infty} \sum_{n=-\infty}^{\infty} C_{mn} e^{jkmd_x \sin\theta \cos\varphi} e^{jknd_y \sin\theta \sin\varphi} \qquad (2)$$

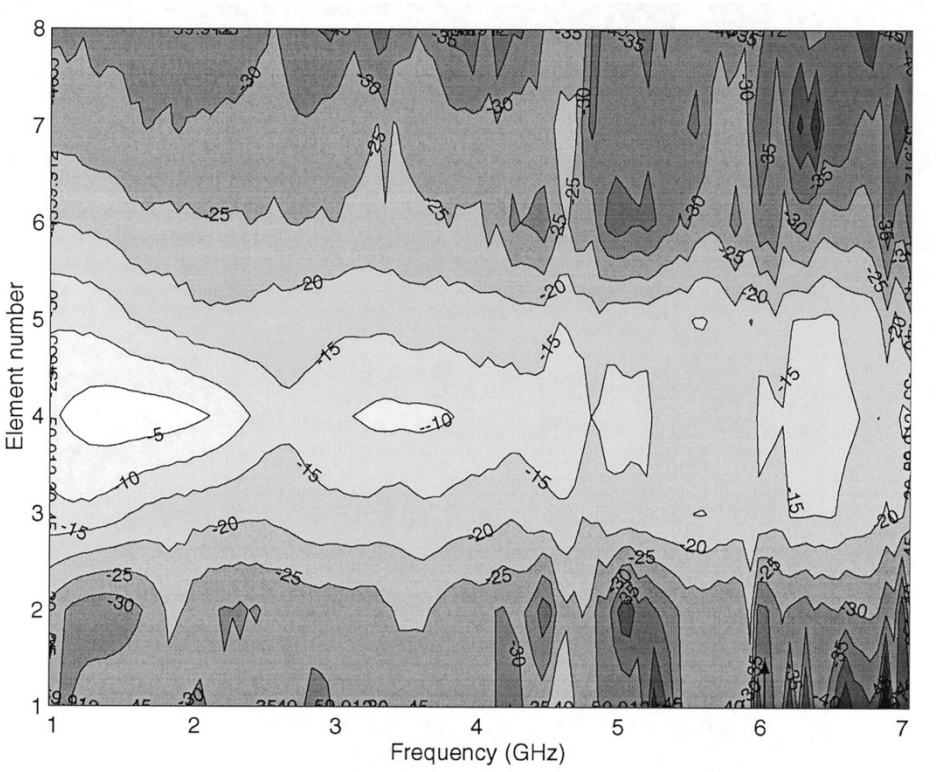

Fig. 7. Magnitude of copolarized mutual coupling coefficient between element 542 and elements 512, 522, 532, 542 (S_{11} is used), 552, 562, 572, and 582 for straight via array. Contour lines at 5 dB each.

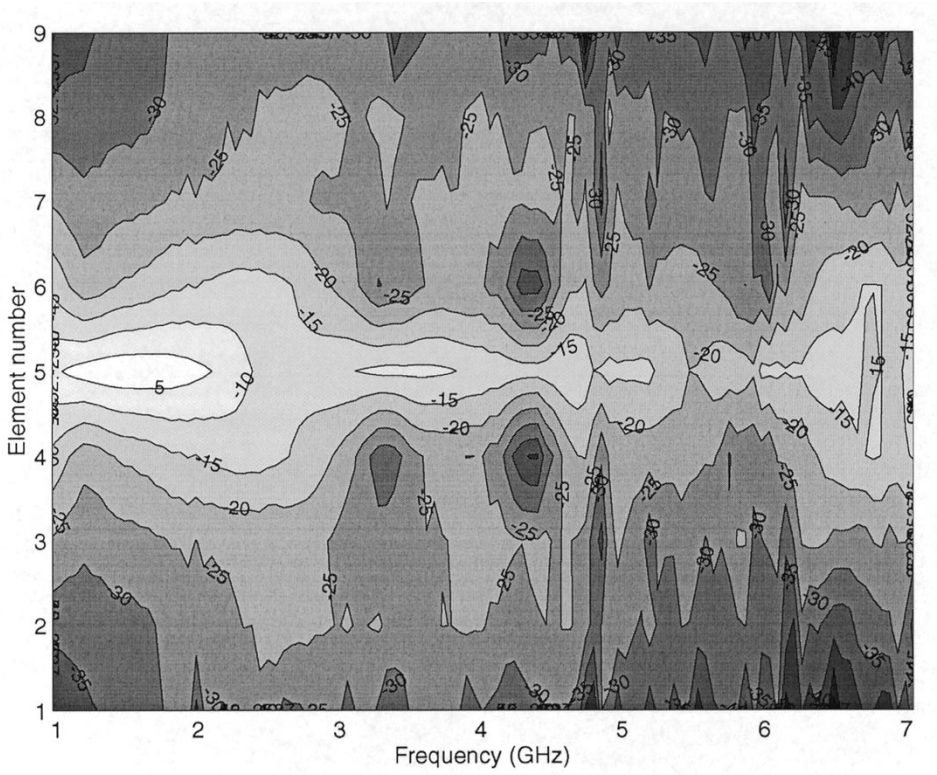

Fig. 8. Magnitude of copolarized mutual coupling coefficient between element 542 and elements 142, 242, 342, 442, 542 (S_{11} is used), 642, 742, 842, and 942 for straight via array. Contour lines at 5 dB each.

is the scan-reflection coefficients, C_{mn} is the mutual coupling coefficient, and d_x and d_y are the dimensions of one rectangular unit cell in the array. Equation (1) is valid if there are no grating lobes and the generator impedance is purely real. Equation (1)

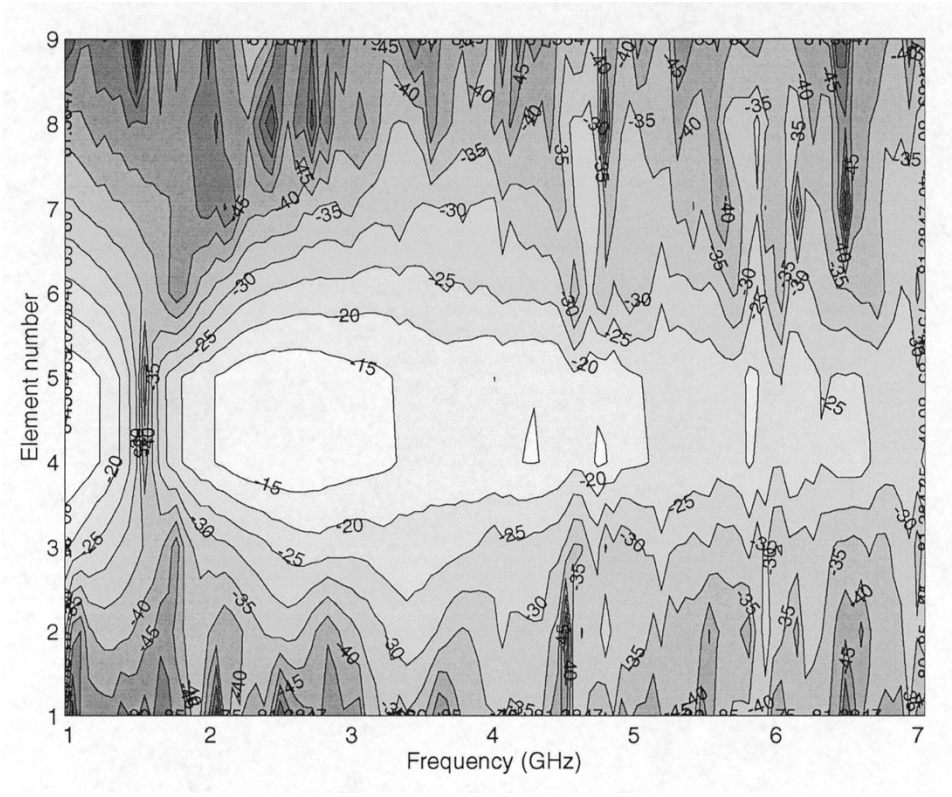

Fig. 9. Magnitude of cross-polarized mutual coupling coefficient between element 542 and elements 511, 521, 531, 541, 551, 561, 571, 581, and 591 for straight via array. Contour lines at 5 dB each.

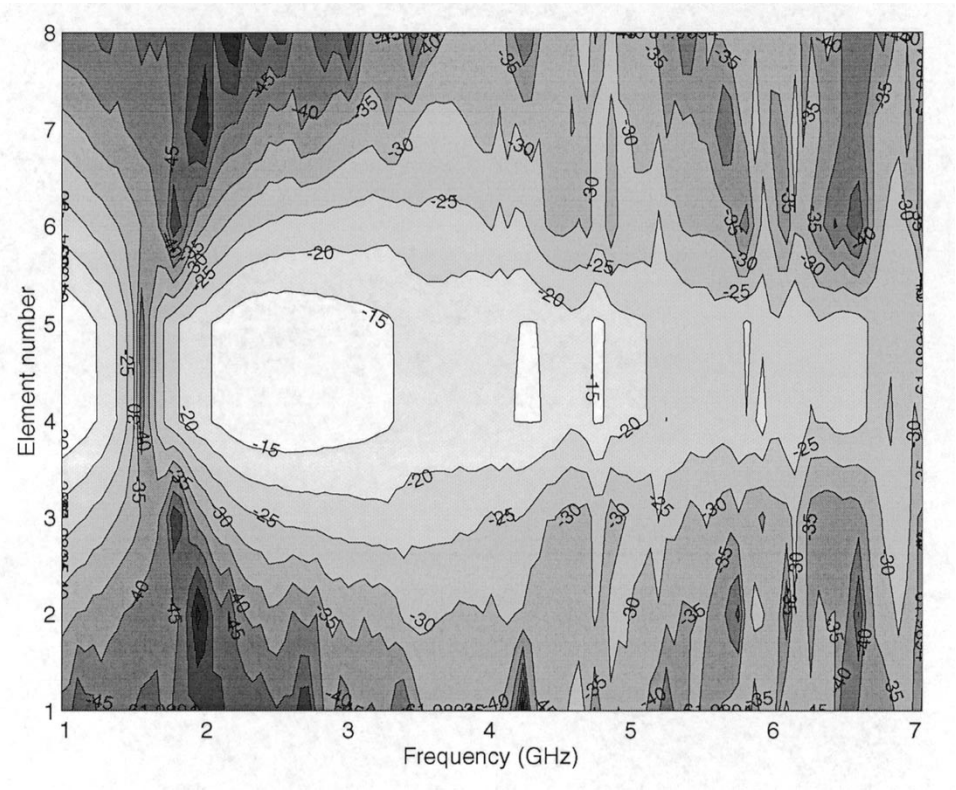

Fig. 10. Magnitude of cross-polarized mutual coupling coefficient between element 542 and elements 141, 241, 341, 441, 541, 641, 741, and 841 for straight via array. Contour lines at 5 dB each.

can be used to approximately calculate the scan-element pattern for finite but large arrays, at least for elements not too close to the array edge. The arrays considered in this paper are not large, but (1) is still used for comparison with the measured

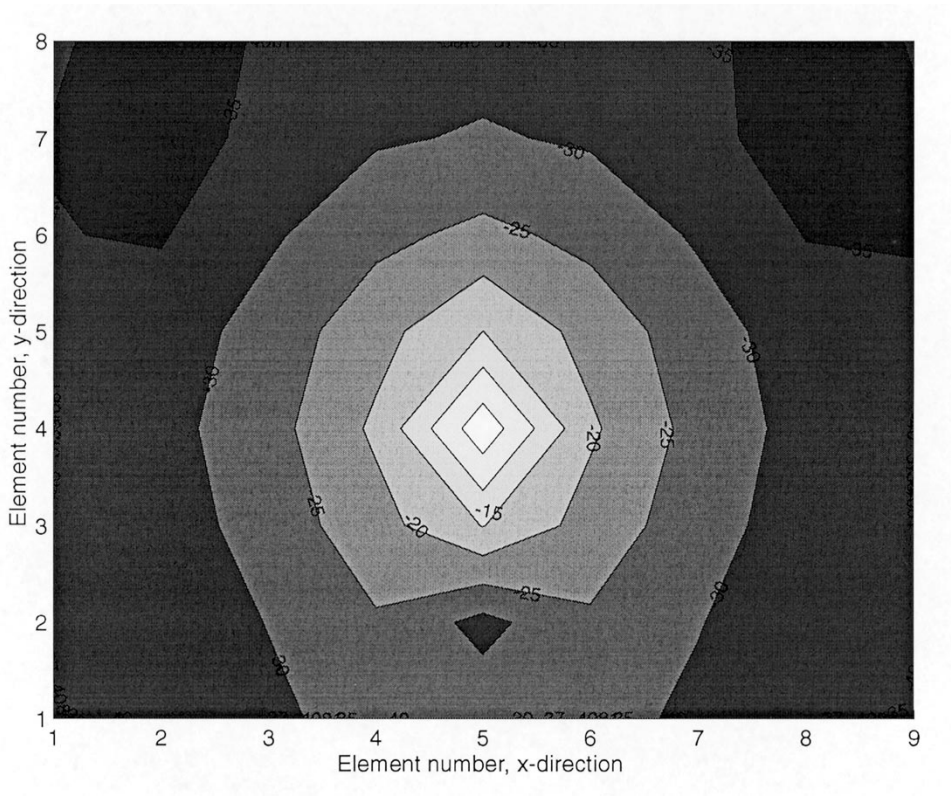

Fig. 11. Magnitude of copolarized mutual coupling coefficient between vertical element 542 and all other vertical elements at 1.5 GHz for straight via array. Contour lines at 5 dB each.

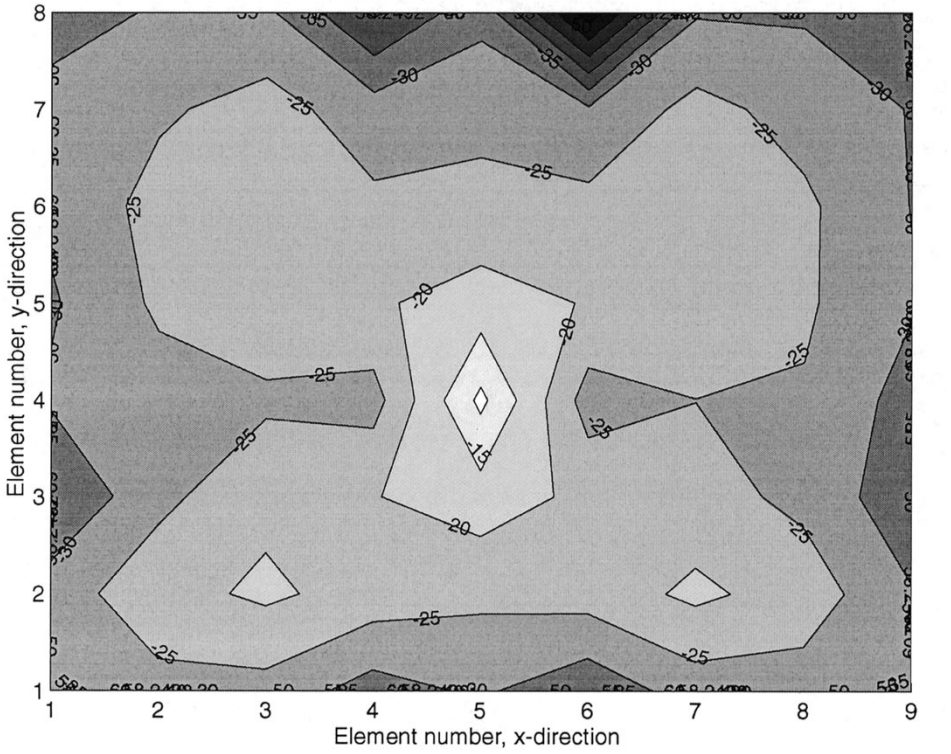

Fig. 12. Magnitude of copolarized mutual coupling coefficient between vertical element 542 and all other vertical elements at 3.5 GHz for straight via array. Contour lines at 5 dB each.

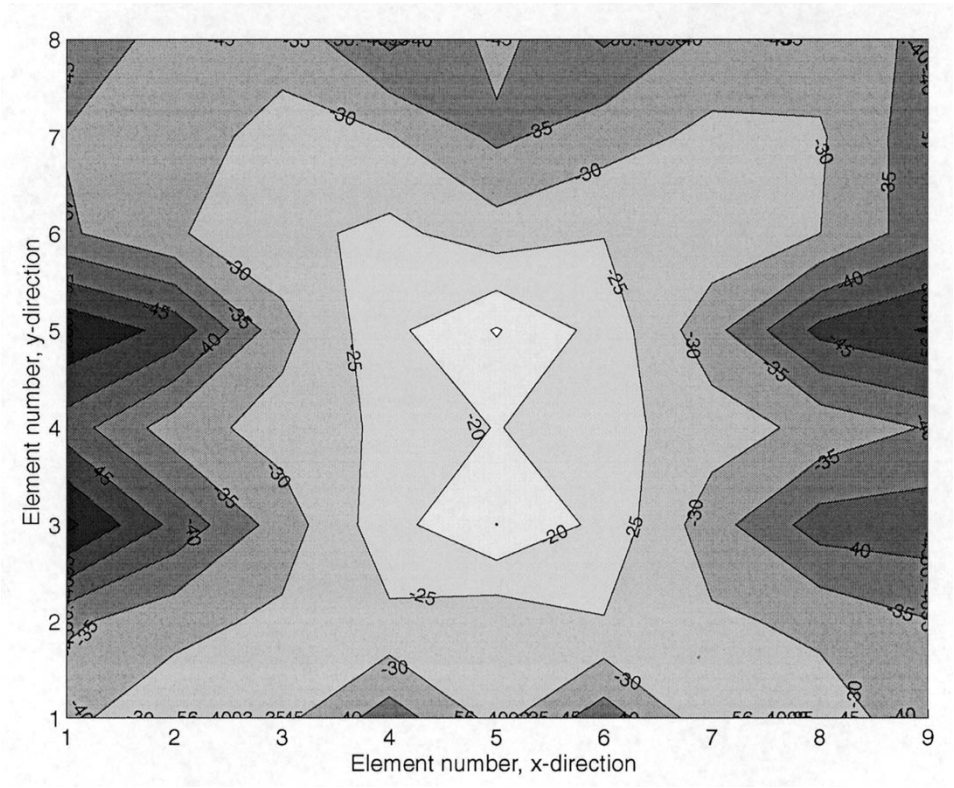

Fig. 13. Magnitude of copolarized mutual coupling coefficient between vertical element 542 and all other vertical elements at 5.5 GHz for straight via array. Contour lines at 5 dB each.

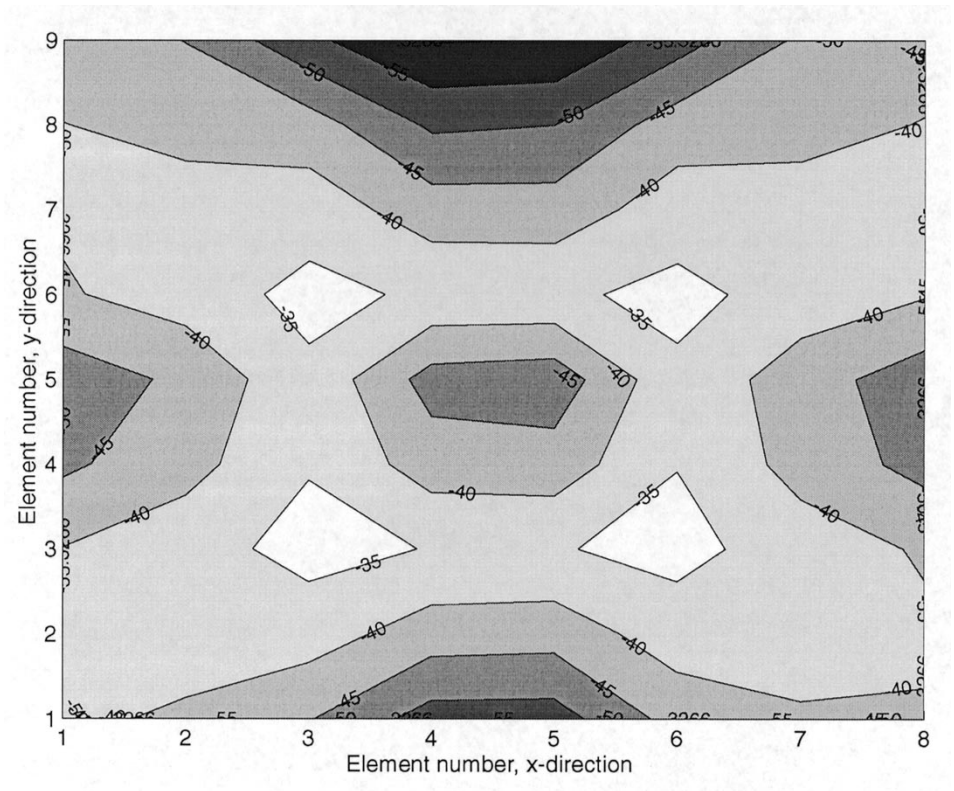

Fig. 14. Magnitude of cross-polarized mutual coupling coefficient between vertical element 542 and all horizontal elements at 1.5 GHz for straight via array. Contour lines at 5 dB each.

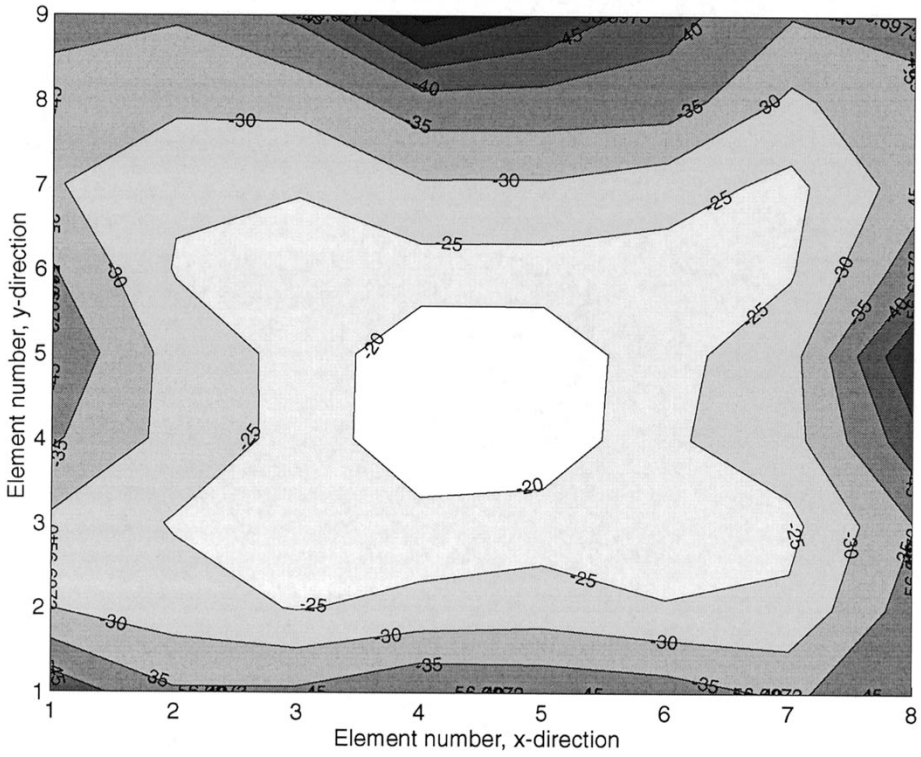

Fig. 15. Magnitude of cross-polarized mutual coupling coefficient between vertical element 542 and all horizontal elements at 3.5 GHz for straight via array. Contour lines at 5 dB each.

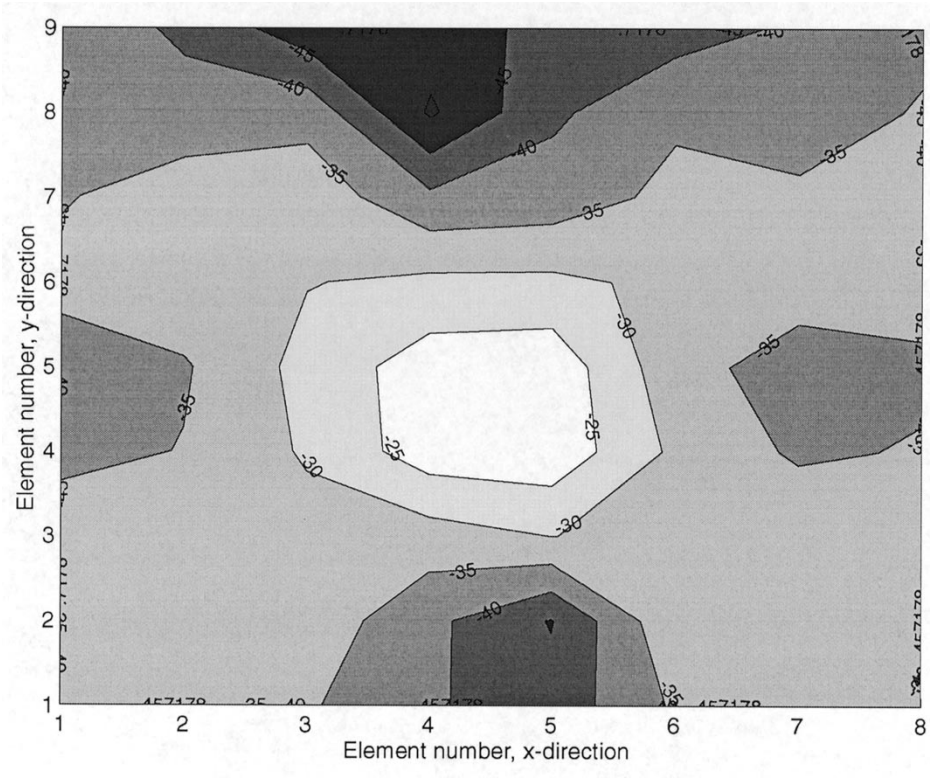

Fig. 16. Magnitude of cross-polarized mutual coupling coefficient between vertical element 542 and all horizontal elements at 5.5 GHz for straight via array. Contour lines at 5 dB each.

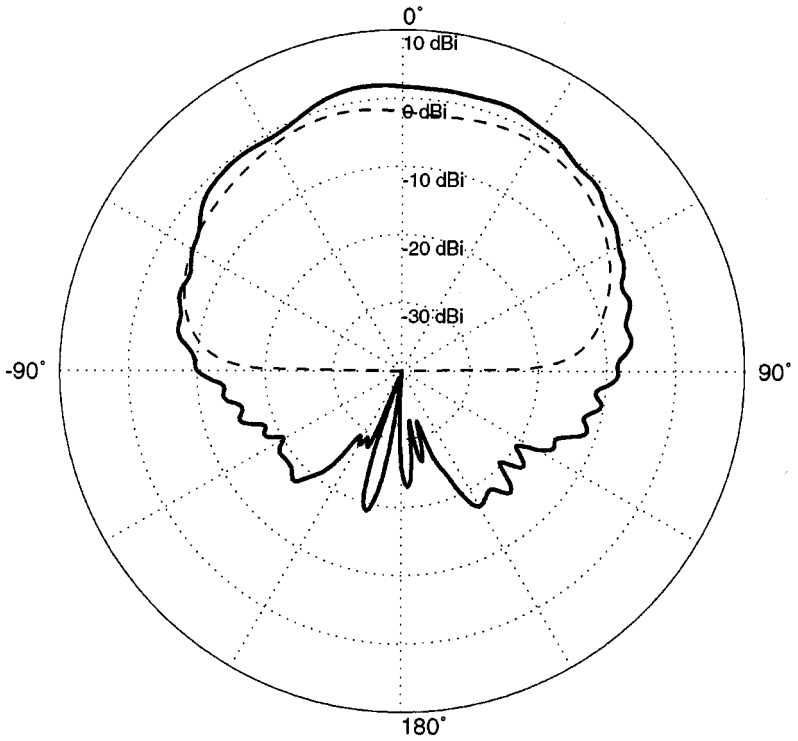

Fig. 17. E-plane scan element pattern (absolute gain) at 3.2 GHz for straight via array. Solid line: measured. Dotted line: calculated from measured mutual coupling coefficients.

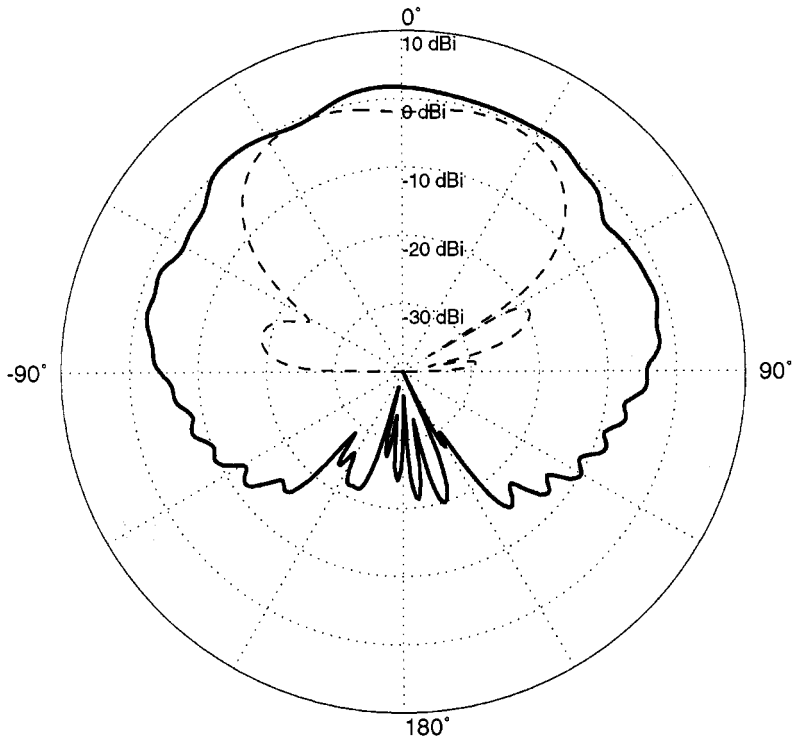

Fig. 18. H-plane scan element pattern (absolute gain) at 3.2 GHz for straight via array. Solid line: measured. Dotted line: calculated from measured mutual coupling coefficients.

scan-element pattern. The difference between the measured and calculated pattern indicates how much the central elements are affected by truncation of the array.

The scan-element pattern was measured for element 542, with all other elements terminated with 50 Ω loads. Patterns in the E-plane and the H-plane at 3.2 and 5.2 GHz are shown in Figs. 17–20. The measured and calculated patterns agree better at 5.2 GHz than at 3.2 GHz. Patterns at other frequencies show the trend of better agreement at higher frequencies. This behavior is expected, since the array becomes electrical larger at

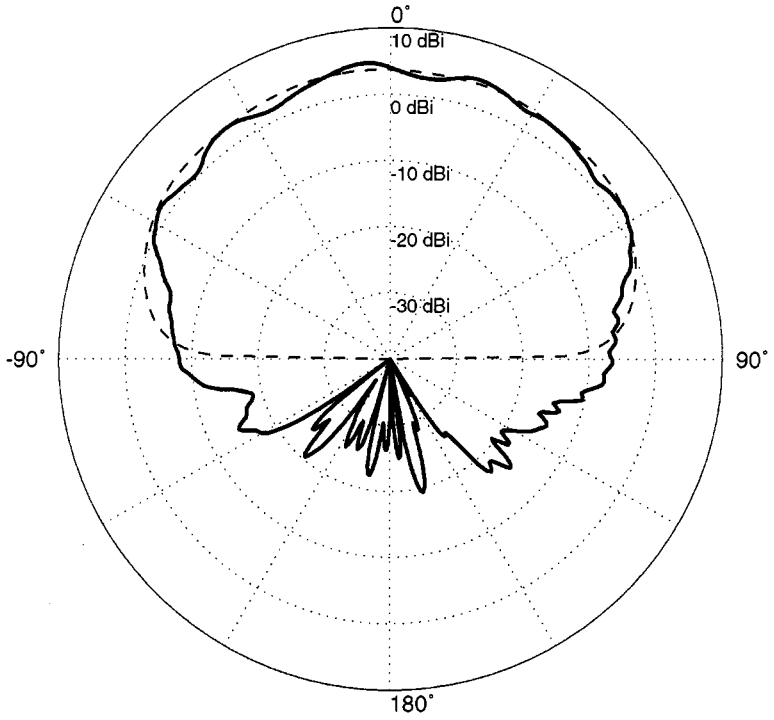

Fig. 19. E-plane scan element pattern (absolute gain) at 5.2 GHz for straight via array. Solid line: measured. Dotted line: calculated from measured mutual coupling coefficients.

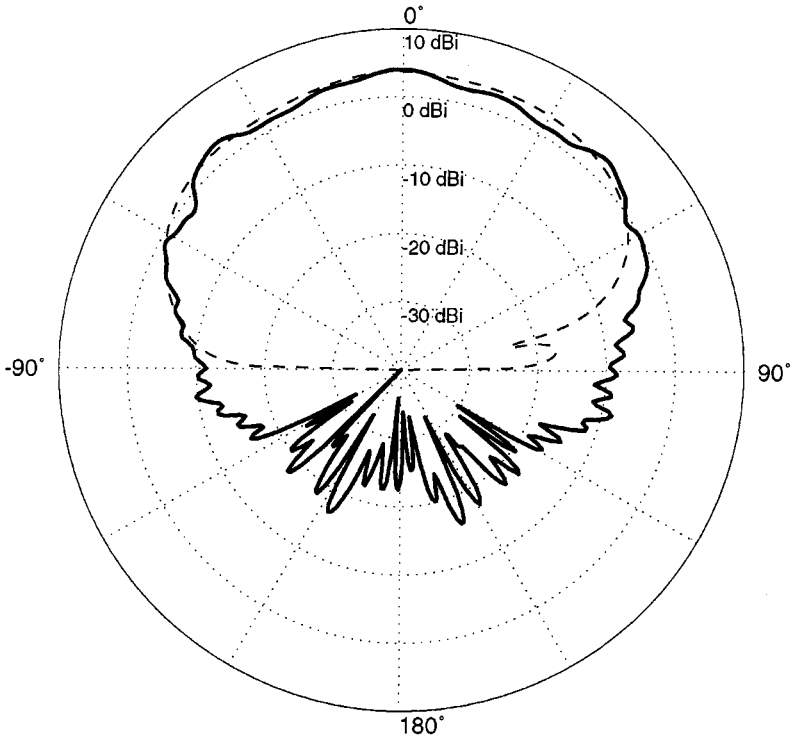

Fig. 20. H-plane scan element pattern (absolute gain) at 5.2 GHz for straight via array. Solid line: measured. Dotted line: calculated from measured mutual coupling coefficients.

higher frequencies. The small oscillations of the measured pattern are typical for finite arrays. Some asymmetry was expected in the E-plane since the element 542 is not in the center of the column. However, it is in the center of its row, so the observed H-plane asymmetry must be caused by manufacturing errors.

VI. Conclusion and Summary

Measured data for two small tapered-slot phased arrays were presented. It was found that because of the strong mutual coupling between distant elements, a dual-polarized array of tapered slot elements designed for wide-angle scanning without

any grating lobes must be electrically large to perform well. Preliminary estimates indicate that it is necessary to use at least 30–40 rows and columns to obtain low-frequency performance that is comparable to infinite array predictions. The resonances, which were predicted by numerical analysis of infinite arrays, were identified by examination of the phase of the mutual coupling coefficients and the use of plated-through vias seems to be adequate to remove most of these resonances from the upper portion of the operating band.

REFERENCES

[1] C. Hemmi, T. Dover, F. German, and A. Vespa, "Multifunction wide-band array design," *IEEE Trans. Antennas Propagat.*, vol. 47, pp. 425–431, Mar. 1999.

[2] M. J. Povinelli, "Wideband dual polarized apertures utilizing closely spaced printed circuit flared slot antenna elements for active transmit and receive phased array demonstration," in *Proc. Antenna Applicat. Symp.*, Allerton Park, IL, 1989.

[3] ——, "Design, performance characterization and hybrid finite element boundary element analysis of a linearly polarized printed circuit tapered notch array," in *Proc. Antenna Applicat. Symp.*, Allerton Park, IL, 1989.

[4] ——, "Experimental design and performance of endfire and conformal flared slot (notch) antennas and application to phased arrays: An overview of development," in *Proc. Antenna Applicat. Symp.*, Allerton Park, IL, 1988.

[5] T-H. Chio and D. H. Schaubert, "Parameter study and design of wide-band widescan dual-polarized tapered slot antenna arrays," *IEEE Trans. Antennas Propagat.*, vol. 48, no. 6, pp. 879–886, June 2000.

[6] T.-H. Chio, D. H. Schaubert, and H. Holter, "Experimental radiation and mutual coupling characteristics of dual-polarized tapered slot antenna (TSA) arrays," in *Proc. Antenna Applicat. Symp.*, Allerton Park, IL, 1999, pp. 280–309.

[7] H. Holter and H. Steyskal, "Broadband FDTD analysis of infinite phased arrays using periodic boundary conditions," *IEE Electron. Lett.*, vol. 35, no. 10, pp. 758–759, May 1999.

[8] ——, "Infinite phased array analysis using FDTD periodic boundary conditions-pulse scanning in oblique directions," *IEEE Trans. Antennas Propagat.*, vol. 47, pp. 1508–1514, Oct. 1999.

[9] H. Holter, T.-H. Chio, and D. H. Schaubert, "Elimination of impedance anomalies in single- and dual-polarized endfire tapered slot phased arrays," *IEEE Trans. Antennas Propagat.*, vol. 48, pp. 122–124, Jan. 2000.

[10] D. H. Schaubert and T.-H. Chio, "Wideband Vivaldi arrays for large aperture antennas," in *Proc. NFRA Conf. Perspectives on Radio Astronomy, Technologies for Large Antenna Arrays*, Dwingeloo, Netherlands, Sept. 1999.

[11] G. J. Wunsch, "Radiation characteristics of dual-polarized notch antenna arrays," Ph.D. dissertation, Univ. Mass., Amherst, Feb. 1997.

[12] N. Amitay, V. Galindo, and C. Wu, *Theory and Analysis of Phased Array Antennas*. New York: Wiley-Intersci., 1972.

[13] R. C. Hansen, *Phased Array Antennas*. New York: Wiley, 1998, pp. 219–222.

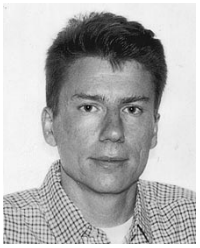

Henrik Holter received the M.S.E.E. degree from the Royal Institute of Technology, Stockholm, Sweden in 1996 with the distinction Best Graduate of the Year, School of Electrical Engineering, and he received the Ph.D. degree in electromagnetic theory from the Royal Institute of Technology in 2000. His research interests include broad-band antenna elements for phased arrays and computational electromagnetics. In 1999, he spent a six-month visit at the Antenna Laboratory, University of Massachusetts, Amherst, participating in research on tapered-slot antenna elements for phased arrays. He served the Swedish navy in 1986–1996 with a Lieutenant degree (Swedish "Kapten") in electrical engineering.

Tan-Haut Chio (S'98–M'99), photograph and biography not available at the time of publication.

Daniel H. Schaubert (S'68–M'74–SM'79–F'89), photograph and biography not available at the time of publication.